Hierarchical Porous TiO$_2$ Monolith Prepared Using Cellulose Monolith as Template

Journal:	*Materials Chemistry Frontiers*
Manuscript ID	QM-RES-02-2021-000220.R2
Article Type:	Research Article
Date Submitted by the Author:	10-Mar-2021
Complete List of Authors:	Lyu, Yanting; Osaka University Asoh, Taka-Aki; Osaka University, Department of Applied Chemistry Uyama, Hiroshi; Osaka Univerisity,

SCHOLARONE™
Manuscripts

Hierarchical Porous TiO$_2$ Monolith Prepared Using Cellulose Monolith as Template

Yanting Lyu, [a] Taka-Aki Asoh *[a] and Hiroshi Uyama *[a]

The photocatalytic process using TiO$_2$ materials under UV light illumination has shown great advantages in wastewater treatment. However, it is necessary to recover the catalyst from the suspension, and the small particle size of the catalyst can cause secondary pollution. Hierarchically porous TiO$_2$ monolithic materials are potential candidates for water remediation, as they are easy to recover and can be used in flow systems. In this study, we used an ecofriendly cellulose material as a template to prepare a hierarchically porous TiO$_2$ monolith. The cellulose monolith template was prepared from cellulose acetate by a thermally induced phase separation method. A composite monolith was then prepared in the presence of the cellulose monolith by a typical sol–gel reaction of titanium isopropoxide (TTIP). This composite monolith was then converted to a TiO$_2$ monolith by burning in air to remove the cellulose monolith. Owing to the hierarchically porous structure of the cellulose monolith template, the obtained TiO$_2$ monolith showed a similar hierarchically porous structure, as confirmed by scanning electron microscopy and nitrogen adsorption–desorption analyses. The pore structure could be controlled by changing the fabrication parameters, such as the type of cellulose monolith and TTIP content. The photocatalytic performance of the TiO$_2$ monolith was evaluated by studying its effect on the degradation of methylene blue (MB) in flow system.

Introduction

A variety of chemical substances, such as dyes, detergents, pesticides, organochlorines, and aromatic hydrocarbons, enter water bodies and cause water pollution.[1, 2] Among several water remediation methods, the photocatalytic process based on the use of titanium oxide (TiO$_2$) materials under UV light illumination has shown great advantages in the treatment of wastewater pollutants owing to its ability to decompose almost all organic contaminants with only photoenergy.[3] Typically, the decomposition of organic contaminants in water is performed by the simple addition of TiO$_2$ powder or TiO$_2$-based materials into the contaminated water.[4, 5] TiO$_2$ materials can effectively bind to organic contaminants and are light-absorbing, resulting in a high rate of the photocatalytic reaction. However, the catalyst powders need to be recovered from the suspension after the reaction. Moreover, inorganic powders frequently cause secondary pollution, which has hampered their practical application. To solve these problems, TiO$_2$-polymer composites are potential candidates for water remediation. For example, cellulose/TiO$_2$ monolith,[6] and MS@TiO$_2$@PPy monoliths[7] were prepared as photocatalytic materials. However, polymer-based materials are limited in their applicability due to calcination at temperatures well below 200 °C and are inadequate as catalyst support for many organocatalytic reactions due to dissolving in most organic solvents. For these reasons, hierarchically porous monolithic TiO$_2$ materials are potential candidates for water remediation in flow system.

Hierarchically porous materials have already received much attention in biomedical and environmental applications owing to their high surface area, high pore volume ratios, excellent accessibility to active sites, and enhanced mass transport and diffusion.[8-11] Compared with conventional porous materials with uniform pore dimensions, hierarchical porous materials with well-defined pore dimensions and topologies can offer the combined benefits of each pore size in a single structure. For example, micro-/mesopores possess size or shape selectivity and high surface area for active site dispersion. The macropores act as flow-through channels and can minimize diffusive resistance to mass transport and provide easier access to the active sites.[8, 12] Therefore, hierarchical porous materials show superior properties for flow-through applications and enable fast separation without loss in efficiency and high-throughput screening.[13] Many hierarchical porous materials have been prepared and used in flow system such as cellulose acetate (CA) monolith,[14] and carboxyl multiwalled carbon nanotubes/thermoplastic polyurethane-based (cMWNTs/TPU) composite monoliths.[15]

Such novel interconnected porous TiO$_2$ materials with a 3D network are currently attracting wide interest owing to their excellent physicochemical properties, such as high specific surface area, high chemical, thermal stabilities, and environmental benignity. These properties enable their utilization in wide applications such as water remediation, next-generation solar cells, gas sensing, and lithium/sodium-ion batteries.[4, 16-18] Novel porous TiO$_2$ monoliths with controlled morphology, porosities, and architectures (especially with hierarchical porosity and mesopores in combination with macropores or micropores) are highly desirable owing to their unique structural features.

a. Department of Applied Chemistry, Graduate School of Engineering, Osaka University, 2-1 Yamadaoka, Suita, Osaka 565-0871, Japan.
E-mail: asoh@chem.eng.osaka-u.ac.jp, uyama@chem.eng.osaka-u.ac.jp

Of the numerous methods for the preparation of porous inorganic materials, amphiphilic block copolymer-assisted sol–gel methods have been confirmed to be a particularly promising approach owing to their advantageous features such as low cost, operational compatibility with ambient atmosphere, and easy one-pot processing route.[19] In the sol–ge process, the hydrolysis and condensation reactions of the organic precursors are preferentially incorporated into one of the blocks through hydrogen bonds. Accordingly, reaction conditions are selected to simultaneously form co-continuous structures, resulting in a network structure of inorganic-material skeletons with macropores.[20] Mesoporous phosphate-based glass (MPG) in the P_2O_5-CaO-Na_2O system was synthesized by using a combination of sol–gel chemistry and supramolecular templating.[21] Macroporous α-Al_2O_3 was synthesized by using dicarboxylic acids as porogenes in the sol–gel process.[22] Pudukudy et al. prepared MgO nanoparticles supported nickel and iron catalysts via a facile sol–gel route without the assistance of any surfactants.[23] However, it is difficult to maintain a porous structure because their synthesis often involves a complicated phase separation in sol–gel reactions. The most commonly used synthetic technique for the fabrication of inorganic materials is "nanocasting" (hard templating), where a hierarchical structured polymer is used as a template, followed by carbonization of the composite and subsequent removal of the template.[24-26]

Cellulose monoliths, as a result of their monolithic and hierarchically porous structure, possess several features such as hydrophilicity, easy chemical modification, large surface area, insolubility in water and common organic solvents, and high mechanical strength.[27] Additionally, hierarchically porous cellulose monoliths exhibiting high hydrophilicity and tolerance toward common solvents can be easily fabricated from a cellulose acetate solution by thermally induced phase separation (TIPS).[28] Utilizing the hydrophilic but water-insoluble properties of cellulose monoliths, it is possible to incorporate the TiO_2 precursor into the monolith skeleton during the sol–gel reaction.

Herein, we used an ecofriendly cellulose monolith as a template to prepare a hierarchically porous TiO_2 monolith. The TiO_2 monolith was prepared in the presence of a cellulose monolith via a typical sol–gel reaction of titanium isopropoxide (TTIP). Hydrolysis and condensation reactions of TTIP occurred during the sol–gel process. Finally, the TiO_2 monolith was obtained by burning the composite monolith in air to remove the cellulose template. Owing to the hierarchically porous structure of the cellulose monolith template, the obtained TiO_2 monolith showed a similar hierarchically porous structure. Moreover, the pore structures could be controlled by altering the fabrication parameters such as the type of cellulose monolith and TTIP content. Furthermore, the photocatalytic performance of the TiO_2 monolith was evaluated by analyzing its effect on the degradation of methylene blue (MB).
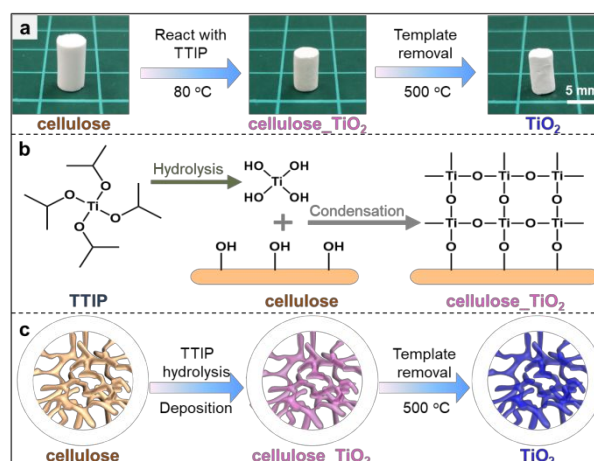
Results and discussion

Fig. 1 (a) The preparation process of TiO_2 monolith. (b) Reaction between TTIP and cellulose monolith. (c) Schematic diagram of preparation of TiO_2 monolith using cellulose monolith as template.

Fig. 1a shows a schematic illustration of the preparation of the TiO_2 monolith using a cellulose monolith as a template. The hierarchically porous cellulose monolith was fabricated according to the TIPS method reported in a previous work.[28] First, the cellulose_TiO_2 monolith was prepared via the sol–gel method and a subsequent reaction of TTIP with the cellulose monolith. After the sol–gel reaction, the cellulose_TiO_2 monolith retained a good columnar shape. The cellulose monolith template was then removed by burning at 500 °C to obtain the TiO_2 monolith. By removing the cellulose, a TiO_2 monolith with a good columnar shape was prepared. The thermal decomposition behavior of the template between 40 and 800 °C was studied by TGA (**Fig. S1**). Usually, the decomposition temperature of a polymer under air is lower than that of under nitrogen. The weight loss of cellulose monolith under nitrogen and air commences at 300 °C and stops around 450 °C. The combustion of the cellulose produced enough energy that the temperature momentarily increased more than the programmed rate, which accounts for the unusual shape of the curve due to the cooling that followed the reactive overheating under air. The weight loss of cellulose_TiO_2 monolith commenced at 300 °C and stopped after 450 °C; however, the TiO_2 monolith did not show any weight loss. Therefore, a burning temperature of 500 °C was sufficient to remove the template.

TTIP is easily hydrolyzed by H_2O molecules. The hydrolysis reaction mechanism between TTIP and H_2O molecules is an SN2 nucleophilic substitution. During the sol–gel method, a condensation reaction also occurs between the hydroxyl groups of cellulose and TTIP (**Fig. 1b**). In the sol–gel process, a solid substrate with hydroxyl groups on its surface is allowed to react with the metal alkoxides in solution to form covalent bonds.[29] Cellulose monoliths possess hydroxyl groups on the surface, and are suitable vehicles for the surface sol–gel process. This means that it is possible to produce a TiO_2 monolith in which the porous structure of the cellulose monolith is transferred by subjecting an appropriate quantity of TTIP to a sol–gel reaction in the presence of the cellulose monolith, followed by the

subsequent removal of the template. Moreover, TiO_2 oligomers and nanoparticles diffuse into the cellulose skeleton, causing cellulose_TiO_2 to form, as shown in **Fig. 1c**. Therefore, when the TTIP content is sufficiently high, the macropore diameter decreases because the amount of TiO_2 covering the skeleton surface increases. The chemical structure of the monolith was studied via XPS and FT-IR analyses. The XPS survey spectrum of cellulose_TiO_2 indicates

the presence of Ti than pure cellulose (**Fig. 2a**). The peaks at 458.4 and 464.3 eV are attributed to the Ti $2p_{3/2}$ and Ti $2p_{1/2}$ of TiO_2 (**Fig. S2a**). The original cellulose monolith displayed two typical peaks at binding energies of 530.4 and 531.0 eV, corresponding to the C–OH bond and C–O–C bond of cellulose, respectively (**Fig. S2b**). Compared with the O 1s spectrum of cellulose, the cellulose_TiO_2 has some additional characteristic signals (**Fig. 2a**). The results obtained from the XPS analysis also suggest the presence of Ti–O–C carbonaceous bonds, which was further supported by the high-resolution O 1s XPS spectra. As shown in **Fig. 2b**, the spectrum can be deconvoluted into three peaks: the peaks at binding energies of 529.8, 531.8, and 534.1 eV can be attributed to the Ti–O–Ti, C–O–Ti, and C–O–C bonds, respectively.[30] As shown in **Fig. 2c**, the FT-IR spectrum of the cellulose monolith features bands at 1023 and ~3400 cm^{-1}, which can be assigned to C–O–C and –OH, respectively.[31] After

the sol–gel process, cellulose_TiO_2 monoliths exhibited bands at 500–800, 1023, and 1632 cm^{-1}, indicating the presence of Ti–O–Ti, C–O–C, and C–O–Ti,[32, 33] and the TiO_2 monoliths show a band at 800–500 cm^{-1}, which can be attributed to the presence of Ti–O–Ti bonds. These results indicate that the prepared TiO_2 can be fixed to the cellulose template because of the condensation reactions between cellulose and TTIP. XRD patterns of cellulose, cellulose_TiO_2, and TiO_2 monoliths are presented in **Fig. 2d**. The pattern of the cellulose monolith has a peak at 2θ = 20.3°. The cellulose_TiO_2 monolith has peaks at 2θ = 25.2, 38.1, 47.9, 54.1, and 63.0°, which can be indexed to the (101), (112), (200), (105), and (204) crystal faces of anatase TiO_2. The TiO_2 monolith also shows peaks consistent with the anatase phase at 2θ = 25.2, 38.1, 47.9, 54.1, 55.1, 63.0, 69.0, 70.4, and 75.3°, which can be indexed to the (101), (112), (200), (105), (211), (204), (116), (220), and (215) crystal faces of anatase TiO_2 (PDF # 001‐004‐0477).[34]

The porous structures of the cellulose, cellulose_TiO_2, and TiO_2 monoliths were examined via SEM (**Fig. 3**). The obtained cellulose_TiO_2 and TiO_2 monoliths possessed a porous structure similar to the hierarchically porous structure of the cellulose monolith. The macropore diameters at each reaction stage were investigated, as shown in **Fig. 3a**. The macropore diameter of the cellulose 80_TiO_2 30 monolith was 7.6 ± 1.7 μm, which
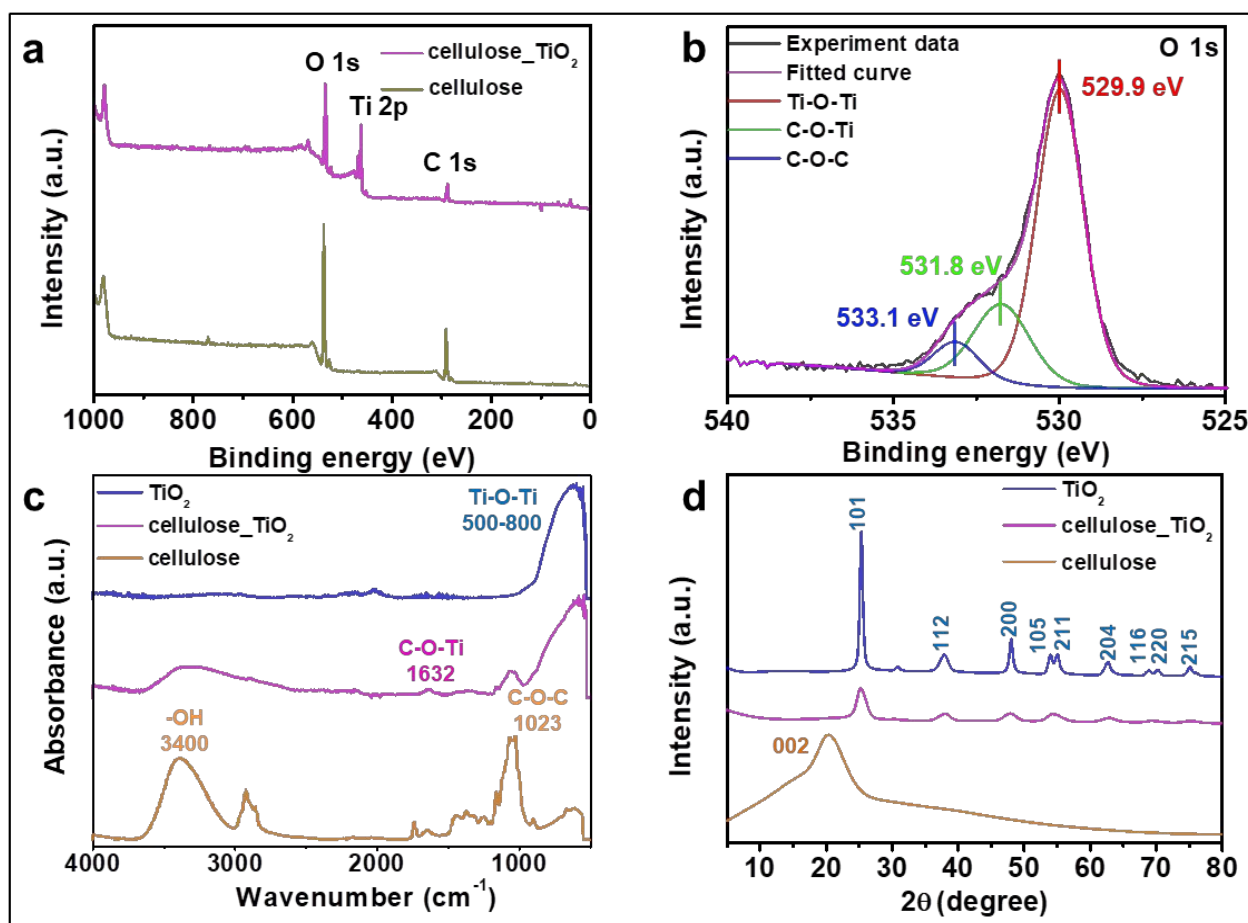

Fig. 2 (a) Survey XPS spectra of cellulose 80 and cellulose 80_TiO_2 40. (b) High-resolution XPS spectra of O 1s of cellulose 80_TiO_2 40. (c) FT-IR spectra and (d) XRD patterns of cellulose 80, cellulose 80_TiO_2 40, and TiO_2 80_40 monoliths.
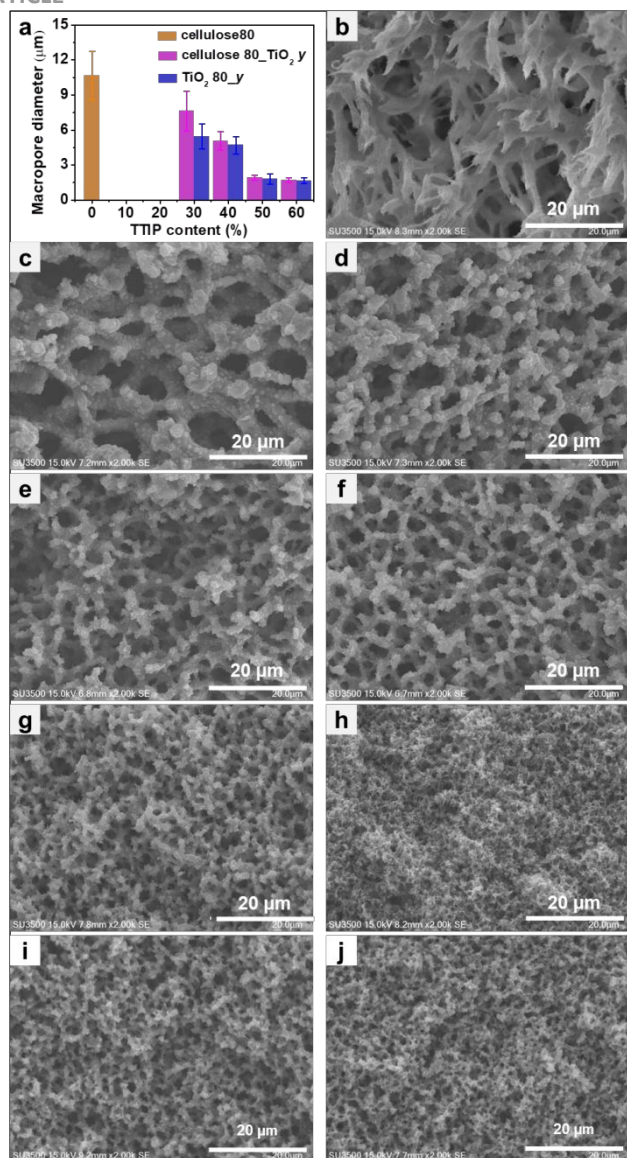
ARTICLE

Fig. 3 (a) Macropore diameters of cellulose, cellulose_TiO$_2$, and TiO$_2$ monoliths prepared with different TTIP contents. SEM images of (b) cellulose 80, (c) cellulose 80_TiO$_2$ 30, (d) TiO$_2$ 80_30, (e) cellulose 80_TiO$_2$ 40, (f) TiO$_2$ 80_40, (g) cellulose 80_TiO$_2$ 50, (h) TiO$_2$ 80_50, (i) cellulose 80_TiO$_2$ 60, and (j) TiO$_2$ 80_60 monoliths.

was smaller than that of the cellulose 80 monolith (10.7 ± 2.1 µm) used as the template. Furthermore, the macropore diameter decreased after the removal of the template, and the TiO$_2$ 80_30 monolith had a macropore diameter of 5.5 ± 1.1 µm. As the TTIP content is considered to affect the amount of TiO$_2$ synthesized, the macropore diameters of the cellulose 80_TiO$_2$ y and TiO$_2$ 80_y monoliths were evaluated as a function of TTIP content by using the same template (cellulose 80). During the calcination process, TiO$_2$ particles were sintered together and porous TiO$_2$ monolith formed. When the TTIP content was less than 20%, after calcination, the prepared TiO$_2$ particles also can be sintered together to form porous structure, however, it is not enough to form a columnar skeleton structure because the amount of TiO$_2$ covering the skeleton surface is not sufficient. As shown in **Fig. 3**, increasing the TTIP content tended to decrease the macropore diameters of cellulose 80_TiO$_2$ y and TiO$_2$ 80_y monoliths. With a TTIP content of 40%, the

macropore diameters of cellulose 80_TiO$_2$ 40 and TiO$_2$ 80_40 monoliths were almost similar, but when the content was increased to 60%, the macropore diameter of TiO$_2$ 80_60 was 1.7 ± 0.3 µm, which was approximately 1/5th of the macropore diameter of the cellulose monolith template. The results indicated that with an increase in the TTIP content, the amount of TiO$_2$ synthesized and attached to the surface of the cellulose monolith increased. Meanwhile, the macropore diameter of the TiO$_2$ 80_y monolith decreased with an increase in the TTIP content.

When the cellulose acetate monolith is a precursor of the cellulose monolith, the pore diameter of the cellulose monolith can be controlled by adjusting the polymer concentration, aging temperature, and solvent composition.[28] In this study, various TiO$_2$ monoliths with different pore diameters were prepared using cellulose monolith templates obtained by varying the polymer concentration was changed when the fixed content of TTIP was 40%. As shown in **Fig. 3a** and **Fig. 4**, with the increase in cellulose acetate concentration, the macropore diameter of the cellulose monolith decreased slightly from 10.7 ± 2.1 µm (cellulose 80) to 1.7 ± 0.2 µm (cellulose 140), but the obtained cellulose x_ TiO$_2$ 40 monoliths maintained the porous structure, and the TiO$_2$ x_40 monoliths also reflected the template structure (**Fig. 4b–j**). These results indicate that the macropore diameter of the TiO$_2$ monolith can be controlled by controlling the macropore diameter of the cellulose monolith template.

For the application of these monoliths as columns, solvent permeability is required. Additionally, the absolute permeability was examined to determine the intensive properties of the monolith in the flow system. The permeability coefficient in the flow system, B0, was measured at a flow rate of 1, 2, 3, 4, and 5 mL/min, and then calculated using the average value. As shown in Table 1, B0 varied depending on the TTIP content and type of cellulose monolith. B0 decreased in the TiO$_2$ monolith prepared with a higher TTIP content and higher cellulose acetate concentration. Hence, all the prepared TiO$_2$ monoliths could be used in the flow system.
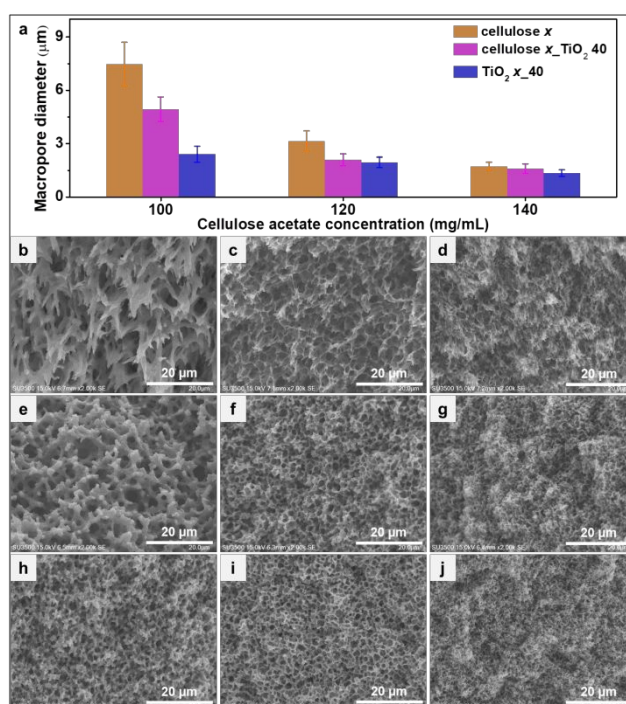

Fig. 4 (a) Macropore diameters of cellulose, cellulose_TiO$_2$, and TiO$_2$ monoliths prepared with different cellulose acetate concentrations. SEM images of cellulose x monolith, cellulose x_ TiO$_2$ 40, and TiO$_2$ x_40 monoliths. x is 100 for (b), (e), and (h); 120 for (c), (f), and (i); and 140 for (d), (g), and (j)

Table 1 BET surface areas, mesopore diameters, pore volumes, B_0, and porosities of TiO$_2$ monoliths

Sample	Surface area (m²/g)	Mesopore diameter (nm)	Pore volume (cm³/g)	B_0 (m²)	Porosity (%)
TiO$_2$ 80_30	64	7.5	0.22	1.7×10^{-11}	89.8
TiO$_2$ 80_40	61	7.5	0.23	3.2×10^{-12}	88.8
TiO$_2$ 80_50	60	7.5	0.24	2.2×10^{-12}	88.9
TiO$_2$ 80_60	64	6.8	0.29	4.7×10^{-13}	87.4
TiO$_2$ 100_40	53	7.5	0.17	1.3×10^{-13}	.87.1
TiO$_2$ 120_40	67	7.5	0.22	2.2×10^{-13}	87.2
TiO$_2$ 140_40	64	7.1	0.22	6.3×10^{-13}	85.9
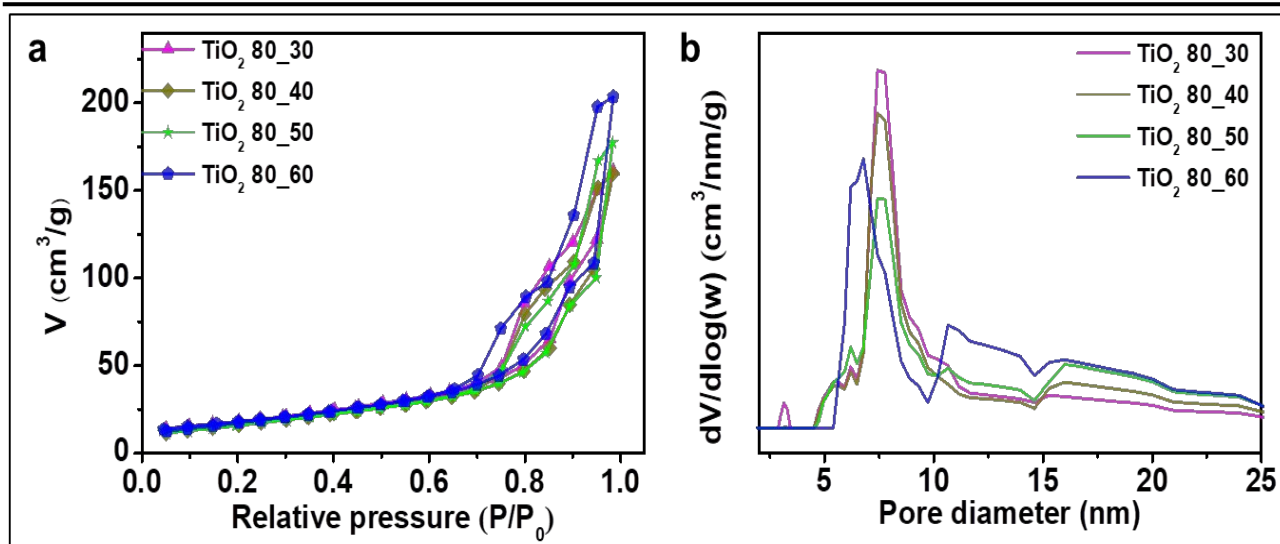
Fig. 5 (a) Nitrogen adsorption–desorption isotherms and (b) corresponding pore size distribution curves of the TiO$_2$ monoliths prepared with different contents of TTIP.
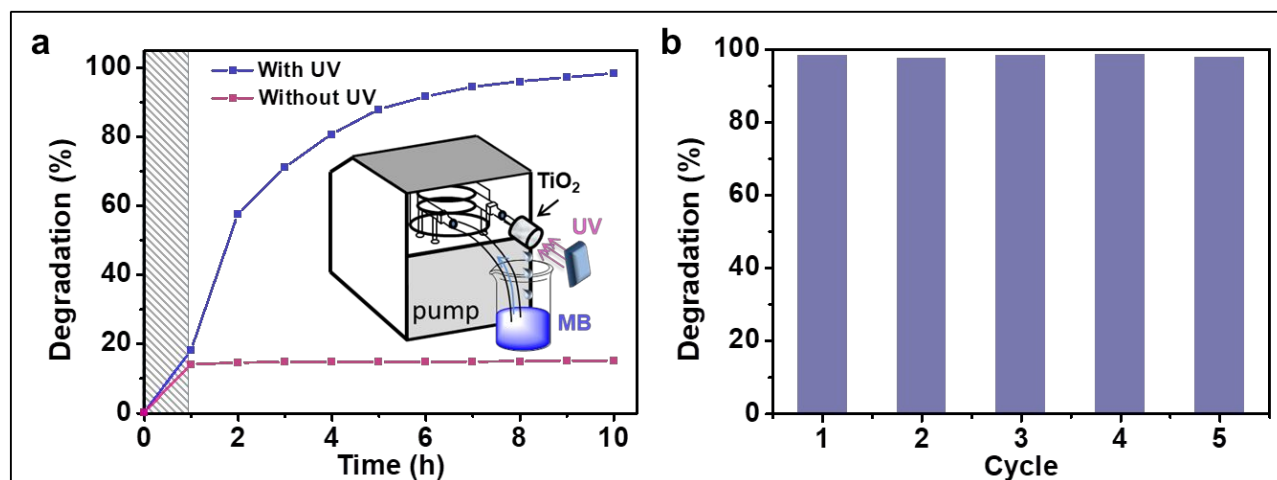
Fig. 6 (a) Photocatalytic activity and adsorption of TiO$_2$ 80_40 monolith for MB solution. Shaded areas indicate periods without illumination (inset is a schematic representation of the experimental setup used for the photocatalytic test). (b) Reusability efficiency of the TiO$_2$ 80_40 monolith after several photocatalytic cycles.

The photocatalytic activity and adsorption results are shown in **Fig. 6** and **Fig.S3**. In batch experiments, 94.5% and 96.2% of the initial dye can be decomposed after 30 min for P25 powders and TiO$_2$ 80_40 powders under UV illumination, respectively. After 60 min, 98.6% and 98.7% of the initial dye can be decomposed for P25 powders and TiO$_2$ 80_40 powders, respectively. The results indicate the prepared TiO$_2$ show high photocatalytic activity (**Fig. S3**). For the circular flow tests, the TiO$_2$ 80_40 monolith (ϕ8 × 7 mm) was fixed in a shrinkable tube and exposed to UV illumination, and the MB solution was flowed circularly through the monolith using a peristaltic pump(EYELA, MP-1000) (**Fig. 6a**, inset). The distance between UV light and monolith is 5 cm. After 1 h, the TiO$_2$ 80_40 monolith can adsorb 14.1% of MB solution; even increase to 10 h, only 15.0% of MB

solution can be adsorbed, the result shown the TiO_2 80_40 monolith reached adsorption saturation after 1 h. For the photocatalytic activity, 91.5% of the initial dye can be decomposed after 5 h under UV illumination. After 9 h of irradiation, 98.2% of the initial dye was decomposed (**Fig. 6a**). The stability of the TiO_2 80_40 monolith was evaluated by recycling experiments. As shown in **Fig. 6b**, after ten successive uses, it can decompose 96.6% of the MB dye. This indicated the good stability and reusability of the TiO_2 monolith.

Experimental

Materials

Cellulose acetate powder (L30) with an acetylation degree of 55% was provided by Daicel Co., Ltd. Japan. TTIP (titanium (IV) isopropoxide), isopropyl alcohol, and MB were purchased from Tokyo Chemical Industry Co., Ltd. Titanium (IV) oxide (P25) was purchased from Fujifilm Wako Pure Chemical Corporation. All the other chemicals used were chemically purified and commercially purchased.

Preparation of TiO_2 monolith

The cellulose monolith was prepared via the TIPS method reported in a previous work.[28] Cellulose acetate (2.0, 2.5, 3.0, and 3.5 g) was dissolved in 10 mL of dimethylformamide (DMF) at 90 °C. Once the cellulose acetate was completely dissolved by stirring, 15 mL of 1-hexanol was added gradually. Subsequently, the mixture was continuously stirred until it became clear and then was transferred into a mold and stored at 20 °C for 6 h to induce phase separation, forming the cellulose acetate monolith. The dried cellulose monolith was then obtained by deacetylation under alkaline conditions (0.5 mol/L NaOH in methanol) for 3 h and vacuum drying. The cellulose monoliths prepared using different concentrations of cellulose acetate were designated as cellulose x monoliths, in which x refers the concentration of cellulose acetate.

The cellulose_TiO_2 monolith was prepared via a sol–gel reaction in the presence of a cellulose monolith. TTIP was added to isopropyl alcohol and stirred for 20 min. Then, the cellulose monolith (0.50 g) was immersed in the TTIP/isopropyl alcohol solution. Subsequently, deionized water was added to the mixture under vigorous stirring. The volume ratio of isopropyl alcohol to water was 1:10. The solution was subsequently heated to 80 °C for 5 h and cooled to room temperature, following which, the cellulose x_TiO_2 y monolith was washed with distilled water and dried at 80 °C, the total volume of the solution after added distilled water is 15 mL, the TTIP content is defined as the ratio of TTIP volume to the total volume of solution, x refers to the concentration of cellulose acetate (mg/mL) and y refers to the content of TTIP (%).The details are shown in **Table S1**. To remove the cellulose monolith, the cellulose_TiO_2 monolith was calcinated in air (heating from room temperature to 500 °C at a rate of 1 °C/min), maintained at 500 °C for 2 h, and then cooled to room temperature to prepare the TiO_2 x_y monolith.

Characterization

Fourier transform infrared (FT-IR) measurements of the samples were performed using a Thermo Scientific Nicolet iS5 spectrometer equipped with an iD5 ATR attachment. All spectra were acquired at a resolution of 4 cm^{-1} across 100 scans in the scan range of 4000–500 cm^{-1}. The morphology of the monoliths was investigated via scanning electron microscopy (SEM) by using a Hitachi S-3000N scanning electron microscope operated at 15 kV. The Brunauer-Emmett-Teller (BET) surface area was studied by nitrogen adsorption–desorption analysis (Quantachrome Instruments). Samples were vacuum-degassed at 70 °C for 24 h prior to measurement. The pore diameter distribution and pore volume were obtained using density functional theory (DFT). Thermogravimetric analysis (TGA) was conducted using a thermogravimetric analyzer (Hitachi, STA7200RV) in the temperature range of 40–800 °C at a heating rate of 10 °C/min under nitrogen protection. Powder X-ray diffraction (XRD) patterns were obtained using a SmartLab (Rigaku Corporation, Japan) with a Cu K-beta X-ray source and a scanning speed of 5°/min over a 2θ range of 5–80°. The generator voltage and current were 45 kV and 200 mA, respectively. The elemental compositions of the surfaces were calculated using X-ray photoelectron spectroscopy (XPS, Kratos Ultra 2). For XPS, monochromatic Al Kα was used, and the power of analysis was 75 W (wide) and 150 W (narrow). The survey and high-resolution XPS spectra were collected at fixed analyzer pass energies of 160 eV and 10 eV, respectively. To confirm reproducibility, the measurement was performed three times for each sample. The peaks were fitted using CasaXPS Version 2.3.15 (Casa Software Ltd. Japan).

To measure the permeability of the monolith, it was tightly fitted with a heat-shrink tubing and connected to a digital quantitative tubing pump (As One, DSP-100SA) and digital pressure gauge (Krone, KDM30). The peristaltic pump was employed to allow the water to flow through the monolith. The value of the permeability coefficient, B_0, depends only on the structure of the porous medium. Hence, permeability is regarded as absolute, regardless of the working fluid. Darcy's law defines the equation of permeability in terms of measurable quantities,[3535]

$$B_0 = \frac{L \times v \times \mu}{\Delta P}$$

$$v = \frac{q}{A}$$

where L is the length of the monolith (m), v is the linear velocity of a given fluid in the flow system (m/s), μ is the viscosity of the fluid (Pa·s), ΔP is the pressure drop when an influent flows through the monolith (Pa), q is the flow rate (m^3/s), A is the cross-sectional area of the flow (m^2), and B_0 is the permeability of the porous medium (m^2).

The porosity of the TiO_2 monoliths was evaluated by gravimetric measurement. The porosity was then calculated according to the following equation:

$$\text{porosity} = \left(1 - \frac{\rho_{ap}}{\rho_m}\right) \times 100\%$$

where ρ_m is the density of anatase TiO_2 particles (ρ_m = 3.895 g/cm³), and ρ_{ap} is the density of the prepared TiO_2 monolith.

Photocatalytic tests

The photocatalytic activity of the materials has been evaluated in batch and flow systems. The photocatalytic activity of the TiO_2 powders (TiO_2 monoliths were ground into powder) and P25 powders was tested by studying their effect on the decomposition of MB under UV light in a batch system at room temperature. Monolith pieces (30 mg) and P25 powders (30 mg) were placed in 50 mL of 5 mg/L MB solution under stirring and exposed to UV light LED lamp (λ = 365 nm, 100 mW/cm², PiPhotonics, Inc. HLKK60). Prior to the decomposition experiment, the solution was allowed to flow through the monolith in the dark for 30 min to ensure adsorption–desorption equilibrium, and the concentration was checked regularly. The concentration of MB was checked at different time intervals after centrifugation (14000 rpm, 2 min, Centrifuge MiniSpin plus, Eppendorf, Japan) using a UV-visible spectrophotometer (HITACHI, U-2810)

The photocatalytic activity of the TiO_2 monoliths was tested by studying their effect on the decomposition of MB under UV light in a circular flow system at room temperature. For the tests, the TiO_2 monolith was fixed into a PTFE heat-shrinkable tube to construct a flow system. The reservoir was filled with 25 mL of 5 mg/L MB solution. The MB solution circulated using a peristaltic pump (EYELA, MP-1000) and the flow rate of the pump was set at 3 mL/min. After flow through the monolith, the MB solution was recycled back into the reservoir at room temperature. Prior to the decomposition experiment, the MB solution was allowed to circular flow through the monolith in the dark for 1 h to ensure adsorption–desorption equilibrium, and the concentration was checked regularly. The decomposition was induced by a 25 W UV-LED light irradiation unit with a single peak wavelength of 365 nm (CCS Inc., EFICET-8332A). The concentration of MB was checked at different time intervals using a UV-visible spectrophotometer (HITACHI, U-2810). The decrease in the intensity of the most prominent absorption band of the MB spectra, typically at 664 nm, was analyzed to follow the degradation of the MB solution. After one cycle, the TiO_2 monolith was washed and dried to test its recycling performance. Subsequently, another photocatalytic experiment was conducted as mentioned above. This process was repeated five times. The adsorption capacity of TiO_2 monoliths was tested by using the same method without UV light.

Conclusions

A hierarchically porous TiO_2 monolith was fabricated via the sol–gel method by using a cellulose monolith as a template and TTIP as a raw material. The pore structures were controlled by changing the fabrication parameters, such as the type of cellulose monolith and TTIP content. SEM and nitrogen adsorption–desorption analyses were carried out to evaluate the porous features of the TiO_2 monolith. The BET surface areas of all the TiO_2 monoliths were similar, indicating that increasing

the TTIP content or cellulose acetate concentrations did not affect the surface areas of the TiO_2 monolith. Moreover, owing to their well-formed porous structure, the TiO_2 monoliths possessed a high porosity (approximately 85.9%–89.8%). The TiO_2 monolith exhibited excellent photocatalytic efficiency; the degradation efficiency of MB reached 98.2%. After ten cycles, the monolith also showed a degradation efficiency of more than 96%. Therefore, the TiO_2 monolith was quite stable and reusable. We also believe that the prepared TiO_2 monoliths are promising in other application and further modification. More importantly, this strategy also can be used to prepare other inorganic monolith.

Conflicts of interest

There are no conflicts to declare.

Acknowledgements

References

1.   A. R. Khataee and M. B. Kasiri, Photocatalytic degradation of organic dyes in the presence of nanostructured titanium dioxide: Influence of the chemical structure of dyes, *J Mol Catal a-Chem*, 2010, **328**, 8-26.

2.   M. M. Mekonnen and A. Y. Hoekstra, Global gray water footprint and water pollution levels related to anthropogenic nitrogen loads to fresh water, *Environ Sci Technol*, 2015, **49**, 12860-12868.

3.   K. Nakata, T. Kagawa, M. Sakai, S. Liu, T. Ochiai, H. Sakai, T. Murakami, M. Abe and A. Fujishima, Preparation and photocatalytic activity of robust titania monoliths for water remediation, *Acs Appl Mater Inter*, 2013, **5**, 500-504.

4.   Y. Y. Sheng, J. Yang, F. Wang, L. C. Liu, H. Liu, C. Yan and Z. H. Guo, Sol-gel synthesized hexagonal boron nitride/titania nanocomposites with enhanced photocatalytic activity, *Appl Surf Sci*, 2019, **465**, 154-163.

5.   F. Azeez, E. Al-Hetlani, M. Arafa, Y. Abdelmonem, A. A. Nazeer, M. O. Amin and M. Madkour, The effect of surface charge on photocatalytic degradation of methylene blue dye using chargeable titania nanoparticles, *Sci Rep-Uk*, 2018, **8**.

6.   M. A. Lucchini, E. Lizundia, S. Moser, M. Niederberger and G. Nystrom, Titania-cellulose hybrid monolith for in-flow purification of water under solar illumination, *Acs Appl Mater Inter*, 2018, **10**, 29599-29607.

7.   S. W. Yan, Y. Li, F. Xie, J. Wu, X. H. Jia, J. Yang, H. J. Song and Z. Z. Zhang, Environmentally safe and porous MS@TiO_2@PPy monoliths with superior visible-light photocatalytic properties for rapid oil-water separation and water purification, *Acs Sustain Chem Eng*, 2020, **8**, 5347-5359.

8.   S. Dutta, A. Bhaumik and K. C. W. Wu, Hierarchically porous carbon derived from polymers and biomass: effect of

interconnected pores on energy applications, *Energ Environ Sci*, 2014, **7**, 3574-3592.

9. J. Xiao, D. H. Mei, X. L. Li, W. Xu, D. Y. Wang, G. L. Graff, W. D. Bennett, Z. M. Nie, L. V. Saraf, I. A. Aksay, J. Liu and J. G. Zhang, Hierarchically porous graphene as a lithium-air battery electrode, *Nano Lett*, 2011, **11**, 5071-5078.

10. Z. C. Wu, K. Tian, T. Huang, W. Hu, F. F. Xie, J. J. Wang, M. X. Su and L. Li, Hierarchically porous carbons derived from biomasses with excellent microwave absorption performance, *Acs Appl Mater Inter*, 2018, **10**, 11108-11115.

11. T. Huang, Z. C. Wu, Q. Yu, D. G. Tan and L. Li, Preparation of hierarchically porous carbon/magnetic particle composites with broad microwave absorption bandwidth, *Chem Eng J*, 2019, **359**, 69-78.

12. Z. S. Liu, P. Jiang, G. Huang, X. W. Yan and X. F. Li, Silica monolith nested in sponge (SiMNS): A composite monolith as a new solid phase extraction material for environmental analysis, *Anal Chem*, 2019, **91**, 3659-3666.

13. G. Beck, M. Sieland, J. F. Beleites, R. Marschall and B. M. Smarsly, Independent tailoring of macropore and mesopore space in TiO_2 monoliths, *Inorg Chem*, 2019, **58**, 2599-2609.

14. X. Zhang, B. Wang, X. M. Qin, S. H. Ye, Y. T. Shi, Y. Z. Feng, W. J. Han, C. T. Liu and C. Y. Shen, Cellulose acetate monolith with hierarchical micro/nano-porous structure showing superior hydrophobicity for oil/water separation, *Carbohyd Polym*, 2020, **241**.

15. S. H. Ye, B. Wang, Y. T. Shi, B. Z. Wang, Y. R. Zhang, Y. Z. Feng, W. J. Han, C. T. Liu and C. Y. Shen, Superhydrophobic and superelastic thermoplastic polyurethane/multiwalled carbon nanotubes porous monolith for durable oil/water separation, *Compos Commun*, 2020, **21**.

16. C. X. Chu, J. Yang, Q. Q. Zhang, N. N. Wang, F. E. Niu, X. N. Xu, J. Yang, W. L. Fan and Y. T. Qian, Biphase-interface enhanced sodium storage and accelerated charge transfer: Flower-like anatase/bronze TiO_2/C as an advanced anode material for Na-ion batteries, *Acs Appl Mater Inter*, 2017, **9**, 43648-43656.

17. X. Y. Wang, J. Q. Meng, M. M. Wang, Y. Xiao, R. Liu, Y. G. Xia, Y. Yao, E. Metwalli, Q. Zhang, B. Qiu, Z. P. Liu, J. Pan, L. D. Sun, C. H. Yan, P. Muller-Buschbaum and Y. J. Cheng, Facile scalable synthesis of TiO_2/carbon nanohybrids with ultrasmall TiO_2 nanoparticles homogeneously embedded in carbon matrix, *Acs Appl Mater Inter*, 2015, **7**, 24247-24255.

18. N. Hohn, S. J. Schlosser, L. BieSSmann, S. Grott, S. L. Xia, K. Wang, M. Schwartzkopf, S. V. Roth and P. Muller-Buschbaum, Readily available titania nanostructuring routines based on mobility and polarity controlled phase separation of an amphiphilic diblock copolymer, *Nanoscale*, 2018, **10**, 5325-5334.

19. T. M. Budnyak, I. V. Pylypchuk, V. A. Tertykh, E. S. Yanovska and D. Kolodynska, Synthesis and adsorption properties of chitosan-silica nanocomposite prepared by sol-gel method, *Nanoscale Res Lett*, 2015, **10**.

20. S. S. Yin, L. Song, S. L. Xia, Y. J. Cheng, N. Hohn, W. Chen, K. Wang, W. Cao, S. J. Hou and P. Muller-Buschbaum, Key factors for template-oriented porous titania synthesis: Solvents and catalysts, *Small Methods*, 2020, **4**.

21. F. Foroutan, B. A. Kyffin, I. Abrahams, A. Corrias, P. Gupta, E. Velliou, J. C. Knowles and D. Carta, Mesoporous

phosphate-based glasses prepared via sol-gel, *Acs Biomater Sci Eng*, 2020, **6**, 1428-1437.

22. S. Carstens, C. Splith and D. Enke, Sol-gel synthesis of alpha-Al_2O_3 with enhanced porosity via dicarboxylic acid templating, *Sci Rep-Uk*, 2019, **9**.

23. M. Pudukudy, Z. Yaakob, M. Z. Mazuki, M. S. Takriff and S. S. Jahaya, One-pot sol-gel synthesis of MgO nanoparticles supported nickel and iron catalysts for undiluted methane decomposition into COx free hydrogen and nanocarbon, *Appl Catal B-Environ*, 2017, **218**, 298-316.

24. S. Y. Chen, B. H. Zhou, W. L. Hu, W. Zhang, N. Yin and H. P. Wang, Polyol mediated synthesis of ZnO nanoparticles templated by bacterial cellulose, *Carbohyd Polym*, 2013, **92**, 1953-1959.

25. C. Busuioc, C. D. Ghitulica, A. Stoica, M. Stroescu, G. Voicu, V. Ionita, L. Averous and S. I. Jinga, Calcium phosphates grown on bacterial cellulose template, *Ceram Int*, 2018, **44**, 9433-9441.

26. K. Zhou, P. Yu, X. J. Shi, T. X. Ling, W. N. Zeng, A. J. Chen, W. Yang and Z. K. Zhou, Hierarchically porous hydroxyapatite hybrid scaffold incorporated with reduced graphene oxide for rapid bone ingrowth and repair, *Acs Nano*, 2019, **13**, 9595-9606.

27. Z. T. Xie, T. A. Asoh and H. Uyama, Monolithic cellulose supported metal nanoparticles as green flow reactor with high catalytic efficiency, *Carbohyd Polym*, 2019, **214**, 195-203.

28. Y. R. Xin, Q. C. Xiong, Q. H. Bai, M. Miyamoto, C. Li, Y. H. Shen and H. Uyama, A hierarchically porous cellulose monolith: A template-free fabricated, morphology-tunable, and easily functionalizable platform, *Carbohyd Polym*, 2017, **157**, 429-437.

29. D. H. Yu, X. D. Yu, C. H. Wang, X. C. Liu and Y. Xing, Synthesis of natural cellulose-templated TiO_2/Ag nanosponge composites and photocatalytic properties, *Acs Appl Mater Inter*, 2012, **4**, 2781-2787.

30. Y. F. Sun, J. B. Zhu, L. F. Bai, Q. Y. Li, X. Zhang, W. Tong and Y. Xie, Sandwich-like carbon-anchored ultrathin TiO_2 nanosheets realizing ultrafast lithium storage, *Inorg Chem Front*, 2014, **1**, 58-64.

31. D. S. Lakshmi, N. Trivedi and C. R. K. Reddy, Synthesis and characterization of seaweed cellulose derived carboxymethyl cellulose, *Carbohyd Polym*, 2017, **157**, 1604-1610.

32. W. B. Li, L. F. Li, X. Wu, J. Y. Li, L. Jiang, H. J. Yang, G. Z. Ke, G. Y. Cao, B. Deng and W. L. Xu, High Infrared Blocking Cellulose Film Based on Amorphous to Anatase Transition of TiO_2 via Atomic Layer Deposition, *Acs Appl Mater Inter*, 2018, **10**, 21056-21060.

33. J. Zhao, Y. Q. Gu and J. G. Huang, Flame synthesis of hierarchical nanotubular rutile titania derived from natural cellulose substance, *Chem Commun*, 2011, **47**, 10551-10553.

34. Y. H. Lv, R. H. Yuan, B. Cai, B. Bahrami, A. H. Chowdhury, C. Yang, Y. H. Wu, Q. Q. Qiao, S. Z. Liu and W. H. Zhang, High-Efficiency Perovskite Solar Cells Enabled by Anatase TiO_2 Nanopyramid Arrays with an Oriented Electric Field, *Angew Chem Int Edit*, 2020, **59**, 11969-11976.

35. G. W. Jackson and D. F. James, The permeability of fibrous porous-media, *Can J Chem Eng*, 1986, **64**, 364-374.